PROCEEDINGS OF
THE ROYAL SOCIETY B
BIOLOGICAL SCIENCES

Characterization of the first steps in early shell formation in *Mytilus galloprovincialis*: possible role of tyrosinase

Journal:	*Proceedings B*
Manuscript ID	RSPB-2019-2043.R2
Article Type:	Research
Date Submitted by the Author:	n/a
Complete List of Authors:	Miglioli, Angelica ; University of Genoa, DISTAV; Laboratoire de Biologie du Développement de Villefranche sur mer Dumollard, Remi; Laboratoire de Biologie du Développement de Villefranche sur mer Balbi, Teresa; University of Genoa, DISTAV Besnardeau, Lydia; Laboratoire de Biologie du Développement de Villefranche sur mer Canesi, Laura; University of Genoa, DISTAV
Subject:	Developmental biology < BIOLOGY, Environmental Science < BIOLOGY, Physiology < BIOLOGY
Keywords:	Mytilus, early larval development, shell formation, organic matrix, biomineralization, tyrosinase
Proceedings B category:	Development & Physiology

SCHOLARONE™
Manuscripts

Author-supplied statements

Relevant information will appear here if provided.

Ethics

Does your article include research that required ethical approval or permits?:
This article does not present research with ethical considerations

Statement (if applicable):
CUST_IF_YES_ETHICS :No data available.

Data

It is a condition of publication that data, code and materials supporting your paper are made publicly available. Does your paper present new data?:
My paper has no data

Statement (if applicable):
CUST_IF_YES_DATA :No data available.

Conflict of interest

I/We declare we have no competing interests

Statement (if applicable):
CUST_STATE_CONFLICT :No data available.

Authors' contributions

This paper has multiple authors and our individual contributions were as below

Statement (if applicable):
A.M. designed the research with input from R.D. and L.C.
A.M. and T.B. performed research. R.D. contributed resources. L.C. wrote the paper with con tributions from all authors.

Characterization of the main steps in first shell formation in *Mytilus galloprovincialis*: possible role of tyrosinase

A. Miglioli[1,2], R. Dumollard[2], T. Balbi[1], L. Besnardeau[2] and L. Canesi[1*]

[1]Dipartimento di Scienze della Terra, dell'Ambiente e della Vita, DISTAV, Università di Genova, Corso Europa 26, 16132 Genova, Italy

[2]Laboratoire de Biologie du Developpement de Villefranche-sur-mer, Institut de la mer, Sorbonne Université, CNRS, 181 Chemin du Lazaret, 06230 Villefranche-sur-mer, France

*Corresponding Author
Laura Canesi
DISTAV, University of Genoa
Laura.Canesi@unige.it

Abstract

Bivalve biomineralization is a highly complex and organized process, involving several molecular components identified in adults and larval stages. However, information is still scarce on the ontogeny of the organic matrix before calcification occurs.

In this work, first shell formation was investigated in the mussel *Mytilus galloprovincialis*. The time course of organic matrix and $CaCO_3$ deposition were followed at close times post fertilization (pf) (24, 26, 29, 32, 48 h) by calcofluor and calcein staining, respectively. Both components showed an exponential trend in growth, with a delay between organic matrix and $CaCO_3$ deposition. mRNA levels of genes involved in matrix deposition (chitin synthase-CS; tyrosinase-TYR) and calcification (carbonic anhydrase-CA; extrapallial protein-EP) were quantified by qPCR at 24 and 48 hours pf (hpf) with respect to eggs. All transcripts were upregulated across early development, with TYR showing highest mRNA levels from 24 hpf. TYR transcripts were closely associated with matrix deposition as shown by in situ hybridization (ISH). The involvement of tyrosinase activity was supported by data obtained with the enzyme inhibitor N-Phenylthiourea (PTU). Our results underline the pivotal role of shell matrix in driving first $CaCO_3$ deposition and the importance of tyrosinase in the formation of the first shell in *M. galloprovincialis.*

Keywords: *Mytilus*, early larval development, first shell formation, organic matrix, biomineralization, tyrosinase

Introduction

Biomineralization is a complex physiological process used by a wide range of metazoan species (from sponges to vertebrates, as well as calcifying algae) (1). Within the phylum Mollusca, many species are characterized by the ability to build protective shells made of different $CaCO_3$ polymorphs (2, 3). Although the physiology of early biomineralization in mollusks has been widely explored (3), less is known on the steps that precede first $CaCO_3$ deposition.

Most studies on shell formation and composition in mollusks have been focused on bivalves, that are widespread in freshwater, estuarine and marine environments. In bivalve larvae, first shell formation occurs within 48 hours of first development (3). The process starts at the end of gastrulation with the formation of the shell field, the shell secreting embryonic tissue (3, 4). The shell field undergoes a transient invagination followed by evagination. As it spans over the larval body, the shell field secretes an organic matrix that provides a scaffold for mineral deposition during shell morphogenesis (3, 4). The organic matrix is mainly composed of chitin and acidic polysaccharides, proteins and glycoproteins, that have essential roles in different aspects of shell formation, such as $CaCO_3$ nucleation, growth, and choice of polymorphs (5). Chitin is one of the major polysaccharides of larval and adult shells (6-8). The first shell, or prodissoconch I, later growths into the prodissochonch II, discernible by the concentric growth lines (3). The shell field ultimately differentiates into the mantle, the shell forming tissue in adults (3).

The molecular components involved in shell formation have been largely investigated in adults and larval stages of different bivalves (oysters, clams, mussels) (9-23). Transcriptomics and proteomics data have identified several genes that play important roles in the biomineralization process, as well as a number of shell matrix proteins (SMPs). With regards to SMPs, although considerable differences have been found in adult and larval shells, some functional domains are shared by both SMP repertoires (von Willebrand factor type A, chitin-binding, carbonic anhydrase, and acidic domains) (18). However, the role of each component in the transition from the trocophora to the

first shelled embryo, when the blueprint for calcification is first established, are not fully understood. In particular, despite data being available on shell calcification in early larval stages (20-23), and also in relation to ocean acidification (24-25), much less is known about the ontogeny of the organic matrix before calcification occurs (2). Former studies underlined the role of chitin deposition (5-7). More recently, data on oyster larvae suggested a role for tyrosinase in the initial phase of shell formation (26-27). Sequencing of RNA identified changes in different calcification-related ion transporters and SMPs, including tyrosinase, in early larval stages of the Baltic mussel *M. edulis* (from 20 hours post fertilization - hpf) (23).

Here we investigate the first steps of shell formation from the trocophora (at 24 hpf) to the first D-veliger (at 48 hpf) were investigated in *M. galloprovincialis*, a species of ecological and commercial importance in the Mediterranean (28). The time course of organic matrix and calcified shell deposition were monitored by calcofluor and calcein staining, respectively (25). The approach involved quantifying the levels of mRNA transcripts of selected shell genes previously identified as targets for different chemicals that affect first shell formation (29-31) and tyrosinase, as a potential key step in early matrix development. The role of tyrosinase was further investigated by in situ hybridization (ISH) and treatment with the pharmacological inhibitor of tyrosinase activity N-Phenylthiourea (PTU) (32-33).

1. Material and methods

(a) Animal handling and larval rearing

Sexually mature specimens of *M. galloprovincialis* (4-5 cm long), were collected in the Bay of Villefranche-sur-mer (43.682°N, 7.319°E - France) during the spawning season (January-March 2018). Animals were kept and maintained by the Centre de Ressources Biologiques Marines of the institute (CRBM) at the Institut de la Mer de Villefranche (IMEV), where they were acclimatized in flow-through vessels containing 0.2 μm filtered natural seawater Millipore filtered seawater

(MFSW) (pH 8.0-8.2, 38 ppt salinity, 15°C). Spawning was induced by exposure at 28°C in MFSW in individual 200 mL containers. Fertilization and larval growth were carried out as previously described (29-31) (See Supplementary Information). Larvae were grown at a density of 200 larvae mL^{-1}, utilizing 24-well plates for morphological analyses, six well plates for qPCR, and 50 mL cell culture flasks for ISH.

(b) Larval development and shell biogenesis

Shell biogenesis was followed at different hours post fertilization (24, 26, 29, 32 and 48 hpf), by evaluating the growth of both the organic and inorganic shell components using fluorescent dyes as previously described (25). Calcein (Sigma Aldrich, Lyon, France), a calcium-dependent fluorophore, was used for $CaCO_3$ staining of the calcified shell and added to the culture medium (final concentration 1 mM in 0.01% Dimethyl Sulfoxide-DMSO) before the addition of fertilized eggs. Calcofluor white Fluorescent Brightener 28 (Sigma-Aldrich, Lyon, France), a chitin-staining fluorophore, was employed to visualize the organic matrix, and directly added to the single wells on live larvae five minutes before each sampling time (final concentration 0.02 mM in 0.01% DMSO). At each sampling time, larvae were washed three times in MFSW to remove the excess of both dyes before fixation with 4% paraformaldehyde (PFA) in MFSW, and immediately imaged with a Leica TCS SP8 (Leica, France). Calcofluor (UV channel, Exc: 408 nm / Em: 450-490 nm) gave a blue signal for the organic matrix, while calcein (FITC channel, Exc: 488 nm / Em: 520-560 nm) visualized the calcified shell in green. Composite images were 3D rendered and rotated to measure the area (in μm^2) of one valve in each larva stained by calcein and calcofluor by manual drawing using IMAGEJ software (24). Measurements were performed on a total of at least 70 larvae per time-point obtained from five independent parental pairs ($N \geq 12$ for each parental pair).

Experiments were also carried out in the presence of N-Phenylthiourea (PTU), a well-known competitive inhibitor of diphenolase and phenoloxidase enzymes (32), that has been widely utilized to inhibit tyrosinase activities in marine invertebrates including bivalves (33). Fertilized eggs were

exposed to 10 µM PTU (Sigma Aldrich, Lyon, France) (final concentration 10 µM in 0.01% DMSO) and samples were observed from fertilization to 48 hpf. Experiments were performed in three independent parental pairs. Parallel samples were run in the presence of 0.01% DMSO to rule out possible solvent related effects (not shown).

(c) *M. galloprovincialis* tyrosinase sequence analysis

The sequence of a *M. galloprovincialis* tyrosinase (*Mg*-TYR) was obtained by blasting the available sequence of tyrosinase-1 from *M. coruscus* (GenBank: KP757802.1) in *M. galloprovincialis* whole genome shotgun (34). The sequence obtained (GenBank: KV583276.1), corresponded to a partial tyrosinase-like tyr-A3 protein (GenBank: OPL33388.1). The basic characteristics and conserved domains of the amino sequence of *Mg*-TYR were analysed through the SMART tools (http://smart.embl-heidelberg.de/) to confirm the functional activity. *Mg*-TYR cDNA Open Reading Frame (ORF) and deduced amino acid sequence are shown in Fig. S1A. The ORF is composed by 1879 base pairs (bps) and coding for 626 amino acids. The sequence showed a 90% query coverage with the ORF of *Cg-Tyr1* (GenBank: AGZ15753.1), 92% with *C. gigas* putative tyrosinase like-protein tyr-3 (GenBank: EKC35330) and 52% with *M. coroscus* tyrosinase-like protein 1 (GenBank: KP757802), respectively. The catalytic activity of *Mg*-TYR is confirmed by the presence of the two copper binding domains and the six histidine residues included within (35). The sequence also showed a Chitin binding domain type 2. Multiple alignment of the two copper-binding domains (CuA and CuB) between *Mg*-TYR and tyrosinases of other bivalves *M. coroscus* (*Mc-Tyr1*) and *C. gigas* (*Cgi-Tyr1*) are reported in Fig. S1B; conserved histidine residues are indicated in red.

(d) RNA extraction and qPCR

All procedures were carried out as previously described (29-31). Unfertilized eggs (about 24,000 eggs/mL) pooled from at least six females were collected by centrifugation at 400 ×g for 10 min at 4°C, and the resulting pellet was frozen in liquid N_2. After fertilization, larvae were grown in six well plates and collected at 24 and 48 hpf by a nylon mesh (20 μm pore-filter) and washed with artificial sea water-ASW (29-31). Three wells for each stage were pooled in order to obtain approximately 7,000 embryos/replicate. The larval suspension was centrifuged at 800 ×g, 10 min at 4 °C. Larval pellets and unfertilized eggs were lysed in 1 mL of TRI Reagent (Sigma Aldrich, Milan, Italy). Total RNA was further extracted following manufacturer's instructions (Sigma Aldrich, Milan, Italy). RNA concentration and quality were verified using the Qubit RNA assay (Thermo Fisher, Milan, Italy) and electrophoresis using a 1.5% agarose gel under denaturing conditions. First strand cDNA for each sample was synthesized from 1 μg total RNA (29). Primers pairs employed for qPCR analysis are reported in Tab. S1. qPCR reactions were performed in triplicate in a final volume of 15 μL containing 7.5 μL iTaq universal master mix with ROX (BioRad Laboratories, Milan, Italy), 5 μL diluted cDNA, and 0.3 μM specific primers. A control lacking cDNA template (no-template) was included in the qPCR analysis to determine the specificity of target cDNA amplification. Amplifications were performed in a StepOne real time PCR system apparatus using a standard "fast mode" thermal protocol (sample ramp ± 2.2 °C/s) (Thermo Fisher, Milan, Italy). For each target mRNA, melting curves were utilized to verify the specificity of the amplified products and the absence of artefacts. The amplification efficiency of each primer pair was calculated using a dilution series of cDNA (Tab. S1). HEL and EF-α1 were utilized as the best performing combination of reference gene products (EF1/HEL) for data normalization (29). Analyses were performed on at least four independent mRNA samples. Calculations of relative expression of target mRNAs was performed by a comparative CT method (36) using the StepOne software tool (Thermo Fisher, Milan, Italy). Data, obtained from at least

five independent mRNA samples, are reported as relative expression (log2-transformed fold changes) with respect to unfertilized eggs.

(e) In Situ Hybridization (ISH)

Primer pairs of TYR and CS primer pairs for ISH are reported in Tab. S2 and were used to amplify one fragment of cDNA for each gene. PCR products (around 1.5 kilobase-kb) were cloned into a pGEM-T easy vector (Promega, Charbonnières-les-Bains, France). The selected recombinant plasmid was linearized (SpeI and NcoI restriction enzymes, New England BioLabs, Evry, France) and sequenced to check the orientation of the insert. Sense and antisense digoxigenin-labeled RNA probes were synthesized using the DIG RNA labelling mixture (Roche, Meylan, France) and T7/Sp6 RNA polymerase (Promega, Charbonnières-les-Bains, France). The probes were tested on larvae obtained from at least three independent parental pairs for a total of 150 individuals (N=50 for each parental pair) imaged per time point.

The expression pattern of TYR and CS during shell biogenesis in *M. galloprovincialis* larvae at 24, 29, 32 and 48 hpf was investigated by ISH using an adaptation of the protocol already available for ascidian embryos (37, see Methods in Supplementary information). The signals from the antisense/sense probes for TYR and CS in mussel larvae at 24 and 48 hpf are shown in Fig. S2.

(f) Statistics

Morphometrical data were analysed by the nonparametric one-way Kruskal-Wallis test followed by the Tukey's test ($p<0.05$). Data of qPCR were analysed by Mann-Whitney U test. Statistical differences as well regression equations were calculated using GraphPad Prism 5 software (GraphPad Inc.)

2. Results

(a) Identification of the main steps in early shell formation by double calcofuor/calcein staining

The double calcofuor/calcein staining (25) was employed to follow the progressive deposition of organic shell matrix and $CaCO_3$, respectively, at close times post fertilization between the trochophora and D-Veliger stages (24, 26, 29, 32 and 48 hpf). As shown in Fig. 1, at 24 hpf, the trochophora started to secrete the organic matrix; the calcofluor signal (blue) was mainly visible in a saddle shaped area corresponding to the shell field, that at this stage was still partially invaginated (Fig. 1B and Fig. S3A, arrowheads). By this time, no calcein staining was observed, indicating the absence of stable $CaCO_3$ deposition (Fig. 1C and Fig. S3B). At 26 hpf, the shell field was expanded (Fig. S3B) and calcification (green) started from the centre of the forming valve (Fig. 1B-D); the hinge region began to flatten following the progressive evagination of the shell field (Fig. S3A, arrowheads). By 29 hpf, the calcified area occupied a large part of the growing shell, and the organic matrix could still be observed along the external margins of the valve (Fig. 1B and 1D and Fig. S3B). However, no calcification was visible yet in the hinge region that, by this time, had completed the flattening (Fig. 1C and 1D and Fig S3B). At 32 hpf, the body organization changed dramatically, the larva taking the shape characteristic of the early veliger stage (Fig. 1A): the valve were largely calcified, showing the first accretion rings indicative of the progressive $CaCO_3$ deposition (Fig. 1C). The calcified shell overlaid the organic matrix, except for a thin layer along the margins of the valve (Fig. 1D). By 48 hpf, the D-Veliger stage was reached, with the calcified shell covering the whole body of the larva, and showing more evident concentric accretion rings (Fig. 1C and D).

To better evaluate the time course of shell formation, the areas occupied by the matrix and the calcified shell, respectively, were measured in a single valve of each larva at different times pf (Fig. 2 A and 2B, respectively). The results show that the areas occupied by each shell component have a similar exponential trend in growth, with the areas of the organic matrix significantly higher than

208 those of the calcified shell at all times pf (Fig. 2A). Moreover, the ratio of organic matrix/calcified
209 shell showed a decreasing exponential trend at different time points (Fig. 2C).
210
211 (b) Basal mRNA levels of genes involved in shell biogenesis
212 When basal transcription of each gene was first compared in unfertilized eggs (Tab. S3), extremely
213 low mRNA levels were detected for CA and EP, with those for TYR slightly higher. In contrast,
214 higher expression was observed for CS, indicating a significant contribution of mRNA from
215 maternal origin. Transcription of CS did not change at 24 hpf with respect to fertilized eggs;
216 however, a significant increase was observed at 48 hpf (about 5-folds) (Fig. 3). From 24 hpf EP
217 mRNA levels were increased (2,5 folds with respect to eggs) and further upregulated in the
218 transition from the trocophora to the D-veliger, showing up a 11-fold increase at 48 hpf. At both 24
219 and 48 hpf CA was similarly but more strongly upregulated (about 30 and 80 folds with respect to
220 eggs). Interestingly, the most upregulated gene was TYR, with a dramatic increase in transcription
221 at 24 hpf with respect to eggs (about 3700-folds) without further increases at 48 hpf.
222
223 (c) Expression patterns of genes involved in organic matrix synthesis
224 The expression pattern of TYR and CS was further investigated by ISH at 24, 29, 32, 48 hpf (Fig.
225 4), during the organic matrix and calcified shell deposition (Fig. 4A). Expression of TYR was
226 detectable at 24 hpf in a wide area around the shell field (Fig. 4B), At 29 hpf a more distinct
227 expression pattern was observed: although the TYR signal overlapped the growing shell, it was
228 stronger on the margins of the matrix, and barely visible at the centre of calcifying valve (Fig. 4A
229 and 4B). At 32 hpf, TYR expression was concentrated in rounded patches along the growing margin
230 of the shell, and absent in the centre of the calcified areas. In the fully developed first D-veliger
231 stage, at 48 hpf, expression was limited to the margins of the growing valve, and no signal was
232 detectable in the calcified portion of the shell (Fig. 4).

A distinct pattern was observed for CS (Fig 4C). At 24 hpf, expression was low and concentrated in a small area within the shell field. A similar, but stronger signal was detected at 29 hpf, in an area close to the hinge region. At 32 hpf, CS expression expanded along the hinge axis; finally, at 48 hpf, a weaker signal was observed in the same region but no signal on the shell margin was observed.

(d) Effect of tyrosinase inhibition on shell development

The role of tyrosinase was further investigated in larvae treated with N-phenylthiourea (PTU), a well-known synthetic inhibitor of diphenolase and phenoloxidase enzymes (32). (Fig. 5 and Fig. S4 in comparison with control embryos). At 24 hpf, the calcofluor signal was concentrated only within the shell field (Fig. 5A). At 29 hpf, shell matrix deposition and growth were delayed, only a weak calcification was observed, and asymmetric growing valve were observed (Fig. 5B). Such an asymmetry was more evident at 32 hpf in both organic matrix and calcified shell; moreover, the pattern of calcification appeared inhomogeneous and the shell did not show the typical accretion rings (Fig. 5C). At 48 hpf, the larvae did not develop into D-Veligers and the shell showed irregular patches of organic matrix and calcified areas (Fig. 5D). At this stage in particular, a variety of strong shell malformations were noticeable in comparison to control samples (Fig. S4A): irregular calcification patterns (Fig. S4B), valve with asymmetric growth of organic matrix and calcification (Fig. S5C), absence of significant calcification and misshaped matrix (Fig. S4D). The changes induced by PTU were reflected by significant decreases in the areas of both shell matrix and calcified shell in comparison to controls (-30% from 24 hpf and -50% from 29 hpf, respectively, $p \leq 0.001$) that persisted at all later stages (not shown).

3. Discussion

257 The results presented here provide a detailed quali- and quantitive description of both organic and
258 inorganic components of the first shell formed in mussel larvae. These data underline the pivotal
259 role of shell matrix in driving and organizing early $CaCO_3$ deposition and shell growth, providing a
260 first indication for a relationship between tyrosinase and organic matrix formation in mussels.
261 A clear time delay was observed between the secretion of the organic matrix and $CaCO_3$ deposition:
262 calcification followed the expansion of the organic matrix (indicated by the significantly smaller
263 area at all times pf). Moreover, the ratio organic matrix/calcified shell progressively decreased with
264 the shell growth. These data clearly show that the organic matrix is the blueprint onto which
265 calcification occurs from early steps of shell formation.
266 Expression of CS, CA and EP has been previously shown to be affected by exposure to different
267 chemicals and associated with larval malformations in *M. galloprovincialis* (29-31). TYR has been
268 shown to play a role in shell formation of oyster larvae (26, 27) and Baltic mussels (23). When
269 transcription was compared at 24 and 48 hpf with respect to eggs, the results show that all genes
270 were generally upregulated, although to a different extent, across early development, with mRNA
271 levels for CS<EP<CA<TYR.
272 Both CA and EP, whose mRNA levels were extremely low in eggs, were upregulated from 24 hpf,
273 CA in particular, and further increase in transcription were observed at 48 hpf, supporting their role
274 in calcification. As to those genes involved in matrix deposition, CSs are transmembrane
275 glycosyltransferases responsible for the synthesis of chitin that represents a major constituent of
276 larval shell matrix in *M. galloprovincialis* (6). Among the four selected genes, CS showed the
277 highest basal mRNA levels in eggs, and no upregulation was observed at 24 hpf; actually, at this
278 stage the calcofluor signal, specific for β-glucans, and therefore to β-Chitin, the most abundant
279 chitin polymorph in both larvae and adults (6), was limited to the area corresponding to the shell
280 field. A significant upregulation was observed at 48 hpf. In contrast, TYR, from a low expression in
281 fertilized eggs, was the most upregulated gene, with a dramatic increase in transcription as early as

24 hpf. Tyrosinases (EC 1.14.18.1) are type 3 copper proteins, characterized by two copper-binding domains (39). By oxidizing molecules containing phenol groups (such as tyrosine) into reactive o-quinones that then cause cross-links of substrate molecules, tyrosinases participate in various processes such as wound healing, pigment synthesis, host immunity, and insect cuticle sclerotization (32, 40). The role of tyrosinases in shell formation has been investigated in adult and early larval stages of the oysters *Crassostrea gigas* and *C. angulata,* suggesting a close relationship between expression of a *Cgi-tyr1* and a *Ca-tyrA1*, respectively, and early larval shell biogenesis (26, 27). Although several tyrosinase sequences have been described in *Mytilus* spp. (13, 19, 23), these are the first data on the mRNA level and expression pattern of tyrosinase in parallel with evaluation of shell matrix deposition. The results of ISH clearly show that TYR upregulation preceded and subsequently paralleled the growth of the organic matrix from 24 hpf.

In contrast, ISH of CS revealed a much lower and distinct expression pattern, that was progressively concentrated along the hinge axis, and therefore did not correspond to the areas of the growing matrix. Similarly, preliminary data on ISH of EP and CA do not indicate specific transcription patterns related to initial shell morphogenesis (not shown). The results obtained by ISH for TYR and CS are not only in line with qPCR data, pointing at an earlier and stronger upregulation of TYR at 24 hpf, but also underline a distinct expression pattern of the two genes at 29, 32 and 48 hpf. Although these data do not allow us to understand the exact role of each gene in organic matrix deposition, for TYR the early increase in mRNA levels from 24 hpf and their localization suggest a role in early and progressive guiding matrix and shell growth. For CS, the later up-regulation of mRNA transcripts and their localization at the hinge region may reflect a participation in the subsequent steps and in particular, in the differentiation of the hinge.

Inhibition of tyrosinase activity clearly affected matrix deposition since 24 hpf. From 29 to 48 hpf, evident malformations and dramatic alterations of shell calcification and growth were also observed. As in other bivalves, in early mussel larvae tyrosinase activity might be related to some

sort of maturation process of the organic matrix (27, 40), that allows the next calcification step in terms of homogeneous and organized $CaCO_3$ deposition (41). The presence of a chitin binding domain in TYR further supports a physiological role for tyrosinase activity in correct chitin remodeling not only during organic matrix formation, but also in subsequent shell growth and calcification. Different proteins participate in initiating and controlling the nucleation, growth of inorganic crystals, as well as directing crystal growth through molecular recognitions (42, 43). Tyrosinases may be involved in shell matrix formation by cross-linking fibrous proteins rich in reactive quinones to form water insoluble, protease-resistant polymers (26, 27, 32). Other enzymes with potential phenol oxidase activity should be investigated to obtain a comprehensive knowledge of the process of matrix deposition. Sequencing of mussel genome is revealing a very complex organization with high heterozygosity, abundance of repetitive sequences and extreme intraspecific sequence diversity among individuals, resulting in a large variety of transcripts for both immune-related (34, 44) and biomineralization-related genes (19). In this light, the changes in transcription of few gene sequences related to shell formation evaluated in the present study are only indicative of more heterogeneous and complex processes.

It has been recently reported that ocean acidification affects *M. galloprovincialis* larval soft-tissue development, independent from calcification (25). Shell malformations induced by exposure to low pH, in particular shell hinge abnormalities, originate from an incorrect development and growth of the organic matrix, thus affecting the calcification blueprint (25). Overall, the results obtained so far further support the hypothesis that shell calcification essentially takes on the shape of the secreted organic matrix. Knowledge on these processes may help better understanding bivalve development in a global change scenario, in order to identify early signs of impact of different environmental stressors, from ocean acidification and warming to contaminant exposure. Although marine bivalves, living in complex environments such as coastal ecosystems, must have evolved mechanisms to maintain homeostasis for shell formation in response to natural environmental

fluctuations, shell growth is a highly controlled and energy-limited process (24). Understanding the homeostatic limits for larval shell development can provide clues about whether the magnitude and rate of environmental changes will exceed the buffering limits of embryo physiology, as well as predictive tools to identify potentially harmful compounds (45). Different types of emerging contaminants have been shown to affect early shell formation and gene expression in *M. galloprovicialis* (29-31). The results here obtained indicate that genes involved in shell matrix deposition, in particular tyrosinases, may represent significant targets for a number of environmental chemicals in early larval stages of mussels.

Ethics. Number of adult mussels used and duration of stress was minimized.

Authors' contributions. A.M. designed the research with input from R.D. and L.C. A.M. and T.B. performed research. R.D. contributed resources. L.C. wrote the paper with con tributions from all authors.

Competing interests. The authors declare they have no competing interests.

Funding. This research was partly funded by EMBRC-France n° OOV-AAP 2018–2161 MERMAIDS. The experiments performed in R.D. laboratory were financed by an ANR grant (Marine-EmbryoTox project, ANR-14-OHRI-0009-01-1). A.M. was supported by the PhD in Marine Sciences, DISTAV , University of Genoa and by the Observatoire Oceanologique de Villefranche.

Acknowledgements

The authors would like to thank Laurent Gilletta, Alexandre Jean and Régis Lasbleiz and the Centre de Ressources Biologiques Marines of the CRBM-IMEV that is supported by EMBRC-France, whose French state funds are managed by the Agence Nationale de la Recherche (ANR) within the "Investissement d'Avenir" program (ANR-10-INBS-02); the Imaging platform members: Mébarek Temagoult and Sameh Benaicha; the Ascidian BioCell group members: Alex McDougall, Janet Chenevert, Céline Hebras, Isa Gomez and Genia Gazo.

361 **Figure Legends**

362 **Figure 1**

363 Confocal images showing the time course of early shell formation in *M. galloprovincialis* from the
364 trochophora (24 hpf) to the D-Veliger stage (48 hpf) (lateral view). A) brightfield image of the
365 embryo; B) calcofluor fluorescent signal (blue), corresponding to the organic matrix; C) calcein
366 fluorescence signal (green), corresponding to $CaCO_3$ deposition; D) Merged calcofluor, calcein and
367 brightfield images. Scale bars: 10 μm. The secretion of the organic matrix is visible from 24 hpf
368 (blue) followed by calcification (green) at 26 hpf, with a progressive expansion of the organic
369 matrix and deposition of the shell starting from the central part of each valve. At 29 hpf the
370 calcified valves are well developed onto the organic matrix. By 32 hpf calcification reaches the
371 external margins of the organic matrix and expands towards the hinge region. At 48 hpf the whole
372 shell is calcified and completely encloses the larval body.

373

374 **Figure 2**

375 Boxplots of data obtained from measurements of the areas (μm^2) occupied by the shell matrix (A)
376 and calcified shell (B) in mussel larvae from 24 to 32 hpf (single valve measurements per larva).
377 The total number of individuals (from at least 5 parental pairs) analyzed per time point is reported.
378 The two structures show a similar exponential trend in growth, with the area of organic matrix
379 statistically larger than that of the calcified shell at all times pf. Statistical differences at each time
380 pf are reported in panel A: ** = $p \leq 0.01$; *** = $p \leq 0.001$. In C) data are reported showing the
381 exponential decrease in the ratio organic matrix/calcified shell at different times pf.

382

383 **Figure 3**

Basal expression of genes involved in early shell formation in mussel larvae at trocophore (24 hpf) and D-Veliger (48 hpf) stages: chitin synthase (CS), extrapallial protein precursor (EP), carbonic anhydrase (CA), tyrosinase (TYR). Data (mean±SD), reported from the lowest to the highest level of expression, are shown as relative expression (log2-transformed fold changes) with respect to unfertilized eggs. * = $p<0.05$; ** = $p<0.01$; 24 and 48 hpf vs eggs; # = $p<0.05$, ## = $p<0.001$ 24 hpf *vs* 48 hpf.

Figure 4

Expression pattern of TYR and CS in mussel larvae from 24 to 48 hpf evaluated by In Situ Hybridization-ISH. A) brightfield images and merged signals from calcofluor (blue), calcein (green) as in Fig. 1; B) TYR; C) CS. Both genes are involved in organic matrix synthesis but only TYR parallels the expansion of the shell, while CS is localized nearby the hinge region. Scale bar: 10 μm.

Figure 5

Effects of PTU (10 μM) on mussel early shell formation. Brightfield images and merged fluorescence signals of calcofluor and calcein are reported as in Fig. 1. Representative images show decrease in the area occupied by the organic matrix (blue) at 24 hpf, asymmetric valve and almost absent calcification at 29 hpf. Calcification is evident but asymmetric at 32 hpf, patched and dis-homogeneous at 48 hpf. Scale bar: 10 μm. N.B.: Since in PTU-exposed samples lower calcein and calcofluor signals were observed with respect to controls, images were recorded at higher laser voltage.

References

1. Knoll AH. 2003 Biomineralization and evolutionary history. Reviews in Mineralogy and Geochemistry **54**, 329–356. (doi:10.2113/0540329)

2. Furuhashi T, Schwarzinger C, Miksik I, Smrz M, Beran A. 2009 Molluscan shell evolution with review of shell calcification hypothesis. Comparative Biochemistry and Physiology Part B: Biochemistry and Molecular Biology **154**, 351–371. (doi:10.1016/j.cbpb.2009.07.011)

3. Marin F. 2012 The formation and mineralization of mollusk shell. Frontiers in Bioscience **S4**, 1099–1125. (doi:10.2741/s321)

4. Kurita Y, Deguchi R, Wada H. 2009 Early development and cleavage pattern of the japanese purple mussel, *Septifer virgatus*. Zoological Science **26**, 814–820. (doi:10.2108/zsj.26.814)

5. Falini G, Fermani S. 2004 Chitin mineralization. Tissue Engineering **10**, 1–6. (doi:10.1089/107632704322791646)

6. Weiss IM, Schönitzer V. 2006 The distribution of chitin in larval shells of the bivalve mollusk *Mytilus galloprovincialis*. Journal of Structural Biology **153**, 264–277. (doi:10.1016/j.jsb.2005.11.006)

7. Suzuki M, Sakuda S, Nagasawa H. 2007 Identification of chitin in the prismatic layer of the shell and a chitin synthase gene from the japanese pearl oyster, *Pinctada fucata*. Bioscience, Biotechnology, and Biochemistry **71**, 1735–1744. (doi:10.1271/bbb.70140)

8. Yarra T, Gharbi K, Blaxter M, Peck LS, Clark MS. 2016 Characterization of the mantle transcriptome in bivalves: *Pecten maximus*, *Mytilus edulis* and *Crassostrea gigas*. Marine Genomics **27**, 9–15. (doi:10.1016/j.margen.2016.04.003)

9. Arivalagan J, Yarra T, Marie B, Sleight VA, Duvernois-Berthet E, Clark MS, Marie A, Berland S. 2016 Insights from the shell proteome: Biomineralization to adaptation. Molecular Biology and Evolution **34**, 66–77. (doi:10.1093/molbev/msw219)

10. Marie B *et al*. 2012 Different secretory repertoires control the biomineralization processes of prism and nacre deposition of the pearl oyster shell. Proceedings of the National Academy of Sciences **109**, 20986–20991. (doi:10.1073/pnas.1210552109)

11. Liao Z, Bao L, Fan M, Gao P, Wang X, Qin C, Li X. 2015 In-depth proteomic analysis of nacre, prism, and myostracum of *Mytilus* shell. Journal of Proteomics **122**, 26–40. (doi:10.1016/j.jprot.2015.03.027)

12. Gao P, Liao Z, Wang X, Bao L, Fan M, Li X, Wu C, Xia S. 2015 Layer-by-layer proteomic analysis of *Mytilus galloprovincialis* shell. PLOS ONE **10**, e0133913. (doi:10.1371/journal.pone.0133913)

13. Hüning AK *et al*. 2016 A shell regeneration assay to identify biomineralization candidate genes in mytilid mussels. Marine Genomics **27**, 57–67. (doi:10.1016/j.margen.2016.03.011)

14. Marie B, Arivalagan J, Mathéron L, Bolbach G, Berland S, Marie A, Marin F. 2017 Deep conservation of bivalve nacre proteins highlighted by shell matrix proteomics of the Unionoida *Elliptio complanata* and *Villosa lienosa*. Journal of The Royal Society Interface **14**, 20160846. (doi:10.1098/rsif.2016.0846)

15. Song X, Liu Z, Wang L, Song L. 2019 Recent advances of shell matrix proteins and cellular orchestration in marine molluscan shell biomineralization. Frontiers in Marine Science **6**. (doi:10.3389/fmars.2019.00041)

16. Yin H, Ji B, Dobson PS, Mosbahi K, Glidle A, Gadegaard N, Freer A, Cooper JM, Cusack M. 2009 Screening of biomineralization using microfluidics. Analytical Chemistry **81**, 473–478. (doi:10.1021/ac801980b)

17. Freer A, Bridgett S, Jiang J, Cusack M. 2013 Biomineral proteins from *Mytilus edulis* mantle tissue transcriptome. Marine Biotechnology **16**, 34–45. (doi:10.1007/s10126-013-9516-1)

18. Zhao R *et al*. 2018 Dual gene repertoires for larval and adult shells reveal molecules essential for molluscan shell formation. Molecular Biology and Evolution **35**, 2751–2761. (doi:10.1093/molbev/msy172)

19. Malachowicz M, Wenne R. 2019 Mantle transcriptome sequencing of *Mytilus* spp. and identification of putative biomineralization genes. PeerJ **6**, e6245. (doi:10.7717/peerj.6245)

20. Medaković D. 2000 Carbonic anhydrase activity and biomineralization process in embryos, larvae and adult blue mussels *Mytilus edulis* L. Helgoland Marine Research **54**, 1–6. (doi:10.1007/s101520050030)

21. Weiss IM, Tuross N, Addadi L, Weiner S. 2002 Mollusc larval shell formation: amorphous calcium carbonate is a precursor phase for aragonite. Journal of Experimental Zoology **293**, 478–491. (doi:10.1002/jez.90004)

22. Ramesh K, Hu MY, Thomsen J, Bleich M, Melzner F. 2017 Mussel larvae modify calcifying fluid carbonate chemistry to promote calcification. Nature Communications **8**, 1709 (doi: 10.1038/s41467-017-01806-8)

23. Ramesh K, Yarra T, Clark MS, John U, Melzner F. 2019 Expression of calcification-related ion transporters during blue mussel larval development. Ecology and Evolution **9**, 7157–7172 (doi:10.1002/ece3.5287)

24. Ventura A, Schulz S, Dupont S. 2016 Maintained larval growth in mussel larvae exposed to acidified under-saturated seawater. Scientific Reports **6**. (doi:10.1038/srep23728)

25. Kapsenberg L, Miglioli A, Bitter MC, Tambutté E, Dumollard R, Gattuso JP. 2018 Ocean pH fluctuations affect mussel larvae at key developmental transitions. Proceedings of the Royal Society B: Biological Sciences **285**, 20182381. (doi:10.1098/rspb.2018.2381)

26. Huan P, Liu G, Wang H, Liu B. 2013 Identification of a tyrosinase gene potentially involved in early larval shell biogenesis of the Pacific oyster *Crassostrea gigas*. Development Genes and Evolution **223**, 389–394. (doi:10.1007/s00427-013-0450-z)

27. Yang B, Pu F, Li L, You W, Ke C, Feng D. 2017 Functional analysis of a tyrosinase gene involved in early larval shell biogenesis in *Crassostrea angulata* and its response to ocean acidification. Comparative Biochemistry and Physiology Part B: Biochemistry and Molecular Biology **206**, 8–15. (doi:10.1016/j.cbpb.2017.01.006)

28. FAO. 2004 *Mytilus galloprovincialis*. See www.fao.org/fishery/culturedspecies/Mytilusgalloprovincialis/en.

29. Balbi T, Franzellitti S, Fabbri R, Montagna M, Fabbri E, Canesi L. 2016 Impact of bisphenol A (BPA) on early embryo development in the marine mussel *Mytilus galloprovincialis*: Effects on gene transcription. Environmental Pollution **218**, 996–1004. (doi:10.1016/j.envpol.2016.08.050)

30. Balbi T, Camisassi G, Montagna M, Fabbri R, Franzellitti S, Carbone C, Dawson K, Canesi L. 2017 Impact of cationic polystyrene nanoparticles (PS-NH_2) on early embryo

development of *Mytilus galloprovincialis*: Effects on shell formation. Chemosphere **186**, 1–9. (doi:10.1016/j.chemosphere.2017.07.120)

31. Balbi T, Montagna M, Fabbri R, Carbone C, Franzellitti S, Fabbri E, Canesi L. 2018 Diclofenac affects early embryo development in the marine bivalve *Mytilus galloprovincialis*. Science of The Total Environment **642**, 601–609. (doi:10.1016/j.scitotenv.2018.06.125)

32. Chang TS. 2009 An updated review of tyrosinase inhibitors. International Journal of Molecular Sciences **10**, 2440–2475. (doi:10.3390/ijms10062440)

33. Luna-Acosta A, Thomas-Guyon H, Amari M, Rosenfeld E, Bustamante P, Fruitier-Arnaudin I. 2011 Differential tissue distribution and specificity of phenoloxidases from the Pacific oyster *Crassostrea gigas*. Comparative Biochemistry and Physiology Part B: Biochemistry and Molecular Biology **159**, 220–226. (doi:10.1016/j.cbpb.2011.04.009)

34. Murgarella M, Puiu D, Novoa B, Figueras A, Posada D, Canchaya C. 2016 A first insight into the genome of the filter-feeder mussel *Mytilus galloprovincialis*. Plos ONE **11**, e0151561. (doi:10.1371/journal.pone.0151561)

35. Aguilera F, McDougall C, Degnan BM. 2014 Evolution of the tyrosinase gene family in bivalve molluscs: Independent expansion of the mantle gene repertoire. Acta Biomaterialia **10**, 3855–3865. (doi:10.1016/j.actbio.2014.03.031)

36. Schmittgen TD, Livak KJ. 2008 Analyzing real-time PCR data by the comparative CT method. Nature Protocols **3**, 1101–1108. (doi:10.1038/nprot.2008.73)

37. Paix A, Chenevert J, Sardet C. 2011 Localization and anchorage of maternal mRNAs to cortical structures of ascidian eggs and embryos using high resolution In Situ Hybridization. In Methods in Molecular Biology, pp. 49–70. Humana Press. (doi:10.1007/978-1-61779-005-8_4)

38. Clark MS, Thorne MA, Vieira FA, Cardoso JC, Power DM, Peck LS. 2010 Insights into shell deposition in the Antarctic bivalve *Laternula elliptica*: gene discovery in the mantle transcriptome using 454 pyrosequencing. BMC Genomics **11**, 362. (doi:10.1186/1471-2164-11-362)

520 39. Decker H, Tuczek F. 2000 Tyrosinase/catecholoxidase activity of hemocyanins: structural
521 basis and molecular mechanism. Trends in Biochemical Sciences **25**, 392–397.
522 (doi:10.1016/s0968-0004(00)01602-9)

523 40. Andersen SO. 2010 Insect cuticular sclerotization: A review. Insect Biochemistry and
524 Molecular Biology **40**, 166–178. (doi:10.1016/j.ibmb.2009.10.007)

525 41. Sikes Cs, Wheeler Ap. 1986 The organic matrix from oyster shell as a regulator of
526 calcification *in vivo*. The Biological Bulletin **170**, 494–505. (doi:10.2307/1541857)

527 42. Addadi L, Joester D, Nudelman F, Weiner S. 2006 Mollusk shell formation: A source of
528 new concepts for understanding biomineralization processes. Chemistry - A European
529 Journal **12**, 980–987. (doi:10.1002/chem.200500980)

530 43. Chen Y, Feng Y, Deveaux JG, Masoud MA, Chandra FS, Chen H, Zhang D, Feng L. 2019
531 Biomineralization forming process and bio-inspired nanomaterials for biomedical
532 application: A review. Minerals **9**, 68. (doi:10.3390/min9020068)

533 44. Figueras A, Moreira R, Sendra M, Novoa B. 2019 Genomics and immunity of the
534 Mediterranean mussel *Mytilus galloprovincialis* in a changing environment. Fish &
535 Shellfish Immunology **90**, 440–445. (doi:10.1016/j.fsi.2019.04.064)

536 45. Hamdoun A, Epel D. 2007 Embryo stability and vulnerability in an always changing world.
537 Proceedings of the National Academy of Sciences **104**, 1745–1750.
538 (doi:10.1073/pnas.0610108104)

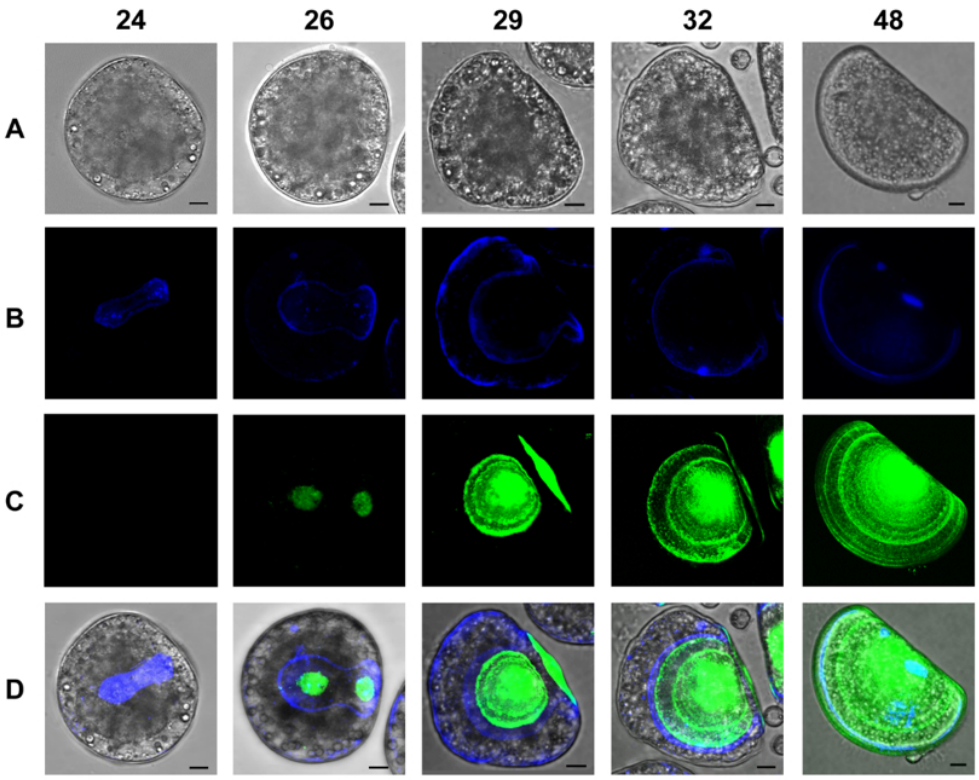

140x110mm (150 x 150 DPI)

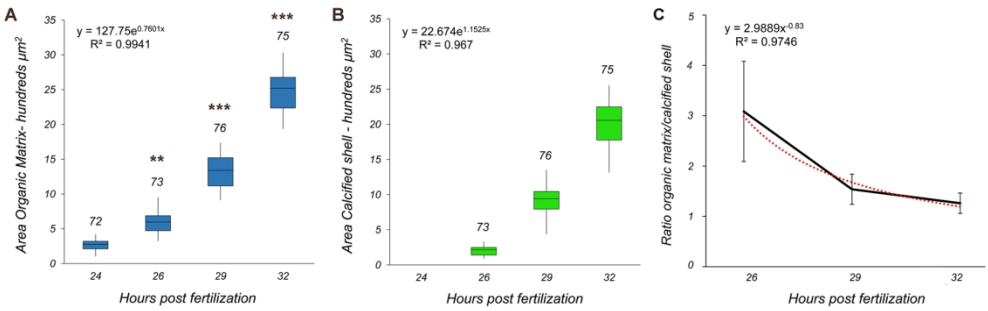
A
y = 127.75e^0.7601x
R² = 0.9941
Area Organic Matrix- hundreds µm²
Hours post fertilization
72
73
76
75
*
**
***
***
B
y = 22.674e^1.1525x
R² = 0.967
Area Calcified shell - hundreds µm²
Hours post fertilization
73
76
75
C
y = 2.9889x^-0.83
R² = 0.9746
Ratio organic matrix/calcified shell
Hours post fertilization

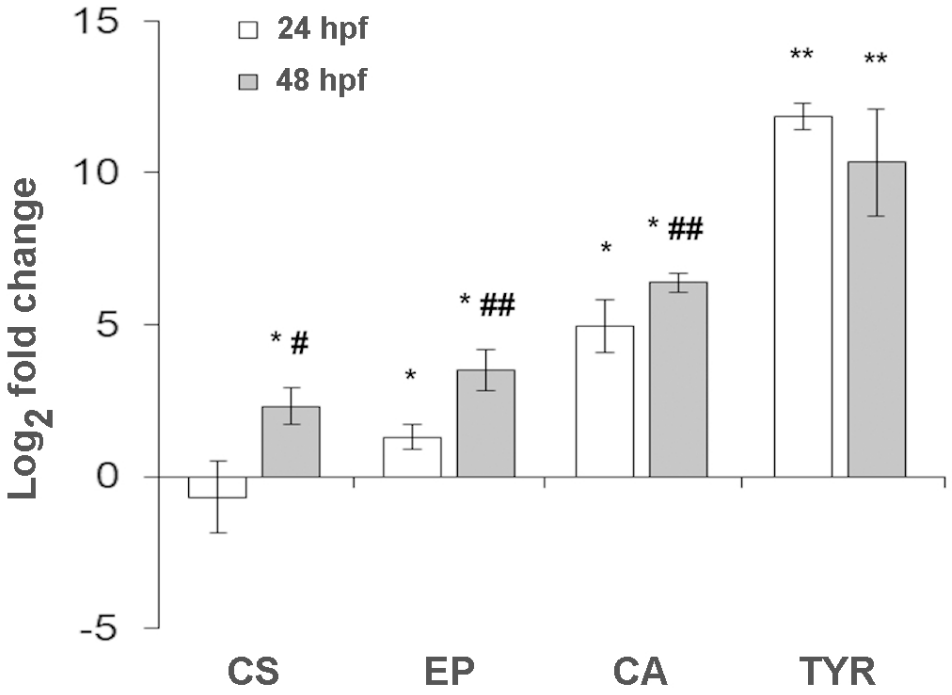
15
10
5
0
-5
Log2 fold change
24 hpf
48 hpf
* #
*
* ##
*
* ##
**
**
CS
EP
CA
TYR

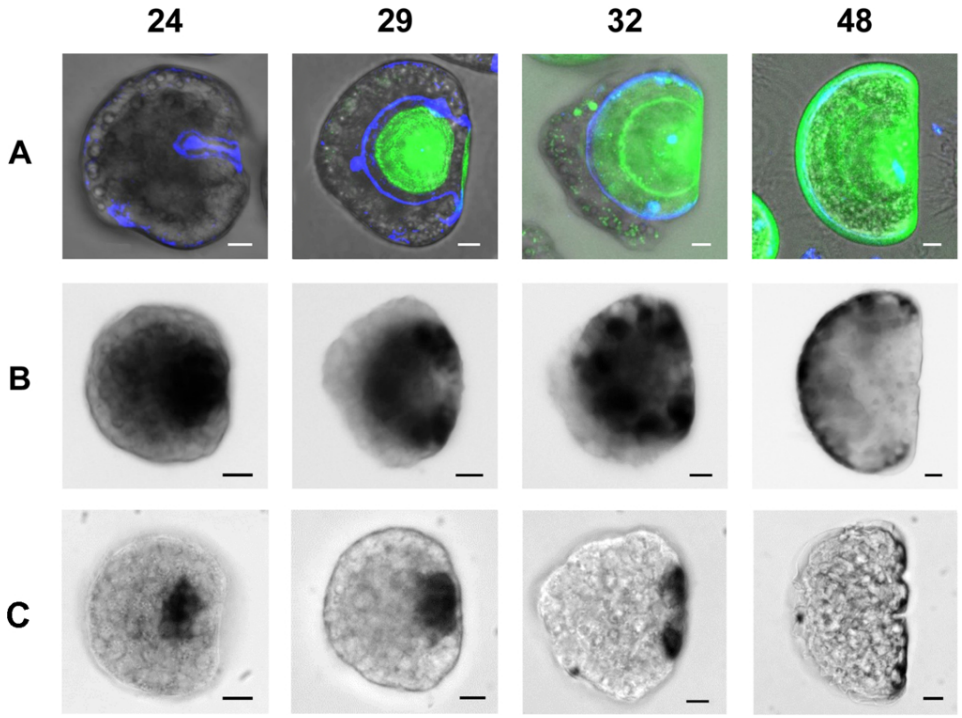

180x132mm (150 x 150 DPI)

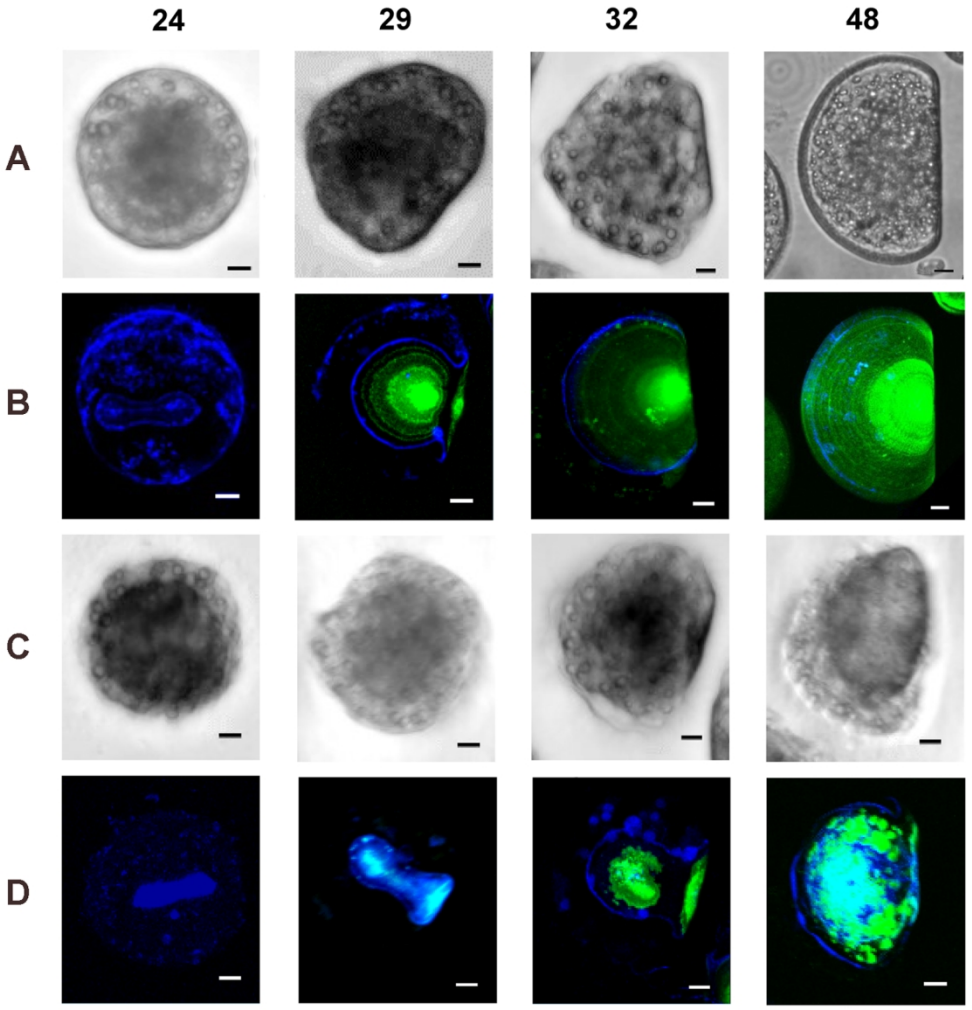

140x144mm (300 x 300 DPI)